

## 15.4 EFFECTS OF REAL-TIME NASA VEGETATION DATA ON MODEL FORECASTS OF SEVERE WEATHER

Jonathan L. Case<sup>1\*</sup>, Jordan R. Bell<sup>2</sup>, Frank J. LaFontaine<sup>3</sup>, and Christa D. Peters-Lidard<sup>4</sup>

<sup>1</sup>ENSCO, Inc./Short-term Prediction Research and Transition (SPoRT) Center, Huntsville, AL

<sup>2</sup>University of Missouri-Atmospheric Science, Columbia, MO

<sup>3</sup>Raytheon/SPoRT Center, Huntsville, AL

<sup>4</sup>NASA Goddard Space Flight Center, Greenbelt, MD

### 1. INTRODUCTION

Since June 2010, the NASA Short-term Prediction Research and Transition (SPoRT) Center has been generating a real-time Normalized Difference Vegetation Index (NDVI) and corresponding Greenness Vegetation Fraction (GVF) composite based on reflectances from NASA's Moderate Resolution Imaging Spectroradiometer (MODIS) instrument. This dataset is generated at 0.01° resolution across the Continental United States (CONUS), and updated daily. The goal of producing such a vegetation dataset is to improve over the default climatological representation of vegetation in land surface and numerical weather prediction models, in order to have better simulations of heat and moisture exchange between the land surface and the planetary boundary layer. Details on how the SPoRT vegetation composites are produced can be found in Case et al. (2011a).

The NASA SPoRT Center at the Marshall Space Flight Center (MSFC) seeks to accelerate the infusion of NASA Earth Science observations, data assimilation, and modeling research into weather forecast operations and decision-making at the regional and local level (Goodman et al. 2004). The SPoRT Center has partnered with and facilitated the use of real-time NASA data to 17 National Weather Service (NWS) Weather Forecast Offices (WFOs) primarily in the Southern Region, as well as private weather entities. Numerous new techniques have been developed to transform satellite and lightning observations (Darden et al. 2010) into useful parameters that better describe changing weather conditions, including proxy products that demonstrate utility for the upcoming GOES-R satellite era (Stano et al. 2012; Fuell et al. 2012).

Vegetation is represented in models by the horizontal and vertical distribution of plant vegetation given by the GVF and Leaf Area Index (LAI), respectively (Gutman and Ignatov 1998). The operational Noah land surface model (LSM; Chen and Dudhia 2001; Ek et al. 2003) within the Weather Research and Forecasting (WRF) model (Skamarock et al. 2008) and National Centers for Environmental Prediction (NCEP) North American Mesoscale (NAM) model (Janjic et al. 2001; Janjic 2003) holds the LAI fixed as a function of vegetation class. The GVF varies spatially according to a global monthly climatology dataset derived from NDVI data on the NOAA Advanced Very High Resolution Radiometer (AVHRR) polar orbiting satellite,

using information from 1985 to 1991 (Gutman and Ignatov 1998; Jiang et al. 2010). Representing data at the mid-point of every month, the monthly climatological dataset is on a grid with 0.144° (~16 km) spatial resolution and is the default dataset within the community WRF model.

A limitation of the climatology is that the annual cycle of GVF is always represented the same in models from year to year. In reality, the response of vegetation to meteorological conditions can vary between seasons and years based on anomalous conditions. Extreme events such as an unusual hard freeze, late bloom due to colder than average temperatures, or drought can lead to a vegetative response that is quite different than the climatological representation. In addition, the dated nature of the GVF climatology and relatively coarse resolution may not be representative of current vegetative conditions in today's high-resolution numerical models. Recent land use changes due to urbanization since the period of record of the GVF climatology likely contribute to mis-representations in the models.

This presentation extends the work of Case et al. (2011a) and complements the companion paper Bell et al. (2012) by examining the impacts of the daily real-time MODIS GVF dataset on model simulations of specific severe weather episodes from 2010 and 2011. Previous studies have also examined the impacts of using real-time GVF in place of the climatology on the Noah land surface model (Miller et al. 2006) and also in severe convective episodes (James et al. 2009).

This study makes use of the NASA-Unified WRF (NU-WRF) system, which is a unification of several NASA modeling capabilities into a single package based on the Advanced Research WRF (ARW). Features of the NU-WRF package include unique Goddard microphysics and short/longwave radiation physics options for the ARW, a Satellite Data Simulator Unit, the Goddard Chemistry Aerosol Radiation and Transport model, the Land Information System (LIS) and companion Validation Toolkit, atmospheric verification, and numerous post-processing capabilities. This study makes use of the coupling between LIS and ARW within NU-WRF to conduct case-study experiments of severe weather events using the climatological GVF versus SPoRT/MODIS GVF data.

Section 2 gives background information on the NASA Land Information System modeling framework within NU-WRF. Section 3 presents the methodology employed for the simulation experiments. Preliminary results are shown in Section 4 followed by a summary and future work in Section 5.

---

\*Corresponding author address: Jonathan Case, ENSCO, Inc., 320 Sparkman Dr., Room 3062, Huntsville, AL, 35805. Email: Jonathan.Case-1@nasa.gov

## 2. NASA LAND INFORMATION SYSTEM

The NASA LIS is a high performance land surface modeling and data assimilation system that integrates satellite-derived datasets, ground-based observations and model reanalyses to force a variety of LSMs (Kumar et al. 2006, 2007). By using scalable, high-performance computing and data management technologies, LIS can run LSMs offline globally with a grid spacing as fine as 1 km to characterize land surface states and fluxes.

Case et al. (2008) presented improvements to simulated sea breezes and surface verification statistics over Florida by initializing the WRF model with land surface variables from an offline LIS spin-up run, conducted on the same WRF domain and resolution. In addition, Case et al. (2011b) demonstrated the utility of using both the LIS land surface fields and high-resolution MODIS SSTs (Haines et al. 2007) to initialize the surface variables over the southeastern U.S., thereby providing a high-resolution lower boundary initial condition over the entire modeling domain that contributed to slight improvements in modeled summertime precipitation systems.

To compare the SPoRT/MODIS to the climatology GVF, the LIS was configured to use the International Geosphere-Biosphere Programme (IGBP) land-use classification (Loveland et al. 2000) as applied to the MODIS instrument (Friedl et al. 2010). All static and dynamic land surface fields were masked based on the IGBP/MODIS land-use classes. The soil properties were represented by the State Soil Geographic (STATSGO; Miller and White 1998) database. Additional required parameters include quarterly climatologies of albedo (Briegleb et al. 1986), a 0.05° resolution maximum snow surface albedo derived from MODIS (Barlage et al. 2005), and a deep soil temperature climatology (serving as a lower boundary condition for the soil layers) at 3 meters below ground, derived from 6 years of Global Data Assimilation System (GDAS) 3-hourly averaged 2-m air temperatures using the method described in Chen and Dudhia (2001).

## 3. SIMULATION EXPERIMENT DESIGN

For these set of experiments, we employed a model configuration mimicking the ARW as run in real-time at the National Severe Storms Laboratory (NSSL) to support the Storm Prediction Center (SPC) and various NWS forecast offices (Kain et al. 2010). The NSSL WRF model runs at 4-km horizontal grid spacing covering the entire CONUS and adjacent portions of northern Mexico, southern Canada, and Pacific/Atlantic Oceans. It is integrated daily for 36 hours from a 0000 UTC initialization time using NCEP NAM initial and boundary conditions. Refer to the following web site for real-time output: <http://www.nssl.noaa.gov/wrf/>.

To provide land surface initialization data, an “offline” LIS spin-up simulation was conducted with 4-km horizontal grid spacing over a CONUS domain identical to the NSSL WRF model configuration. In the offline spin-up run, the Noah LSM was integrated apart from a full NWP model within the LIS framework using

global atmospheric analyses from the NCEP GDAS (Derber et al. 1991) to drive the integration of land surface variables. The offline LIS run was cold-started on 1 June 2008 with a uniform first-guess soil temperature and volumetric soil moisture of 290 K and 25%, respectively, in all soil layers. The Noah LSM was integrated for a time period of 2 years to 1 June 2010, using a time step of 30 minutes. A sufficiently long integration time, or “spin-up”, is necessary to ensure that the model states reach a fine-scale equilibrium with the forcing meteorology acting on the high-resolution input fields (Cosgrove et al. 2003; Rodell et al. 2005). During the two-year spin-up integration, the NCEP GVF climatology was used. After 0000 UTC 1 June 2010, the spin-up run was re-started for two separate offline integrations, a control run that continued using the NCEP GVF, and an experimental run that employed the daily SPoRT/MODIS GVF during the period of study from 1 June through Spring 2011 (illustrated in Figure 1).

Two coupled LIS/ARW simulations within the NU-WRF framework were run out to 36 hours, initialized at 0000 UTC for each case day of interest. Each control coupled simulation was initialized with the NCEP climatological GVFs and land surface fields from the control offline LIS run. Meanwhile, the experimental coupled simulation was initialized with SPoRT/MODIS daily GVFs and land surface data from the experimental offline LIS output that incorporated the SPoRT GVFs. Output of the two different coupled runs were then compared graphically to examine the impacts that the MODIS GVF had on the ARW simulations compared to the GVF climatology dataset.

The severe weather cases simulated include several events from the 2010 and 2011 Spring and Summer. The events simulated include:

- 10-11 June 2010: Colorado supercells,
- 15 June 2010: severe wind episode in the Southeastern U.S.,
- 17 June 2010: tornado outbreak in North Dakota and Minnesota,
- 17 July 2010: Upper Midwest tornadoes and severe wind event,
- 23 July 2010: Vivian, SD record hail event,
- 24-26 October 2010: multi-day severe event and major cyclone across the Southern U.S. and Mississippi Valley,
- 27 April 2011: southeastern U.S. super tornado outbreak,
- 22 May 2011: Joplin, MO EF-5 tornado day,
- 24-25 May, 2011: 2-day tornado and severe weather outbreak from the Southern Plains to the Mississippi Valley.

While the simulations have been made for all these cases, only a small subset of results appears in the paper / presentation as results are still being analyzed.

#### 4. PRELIMINARY IMPACT RESULTS

A general observation on the real-time MODIS GVF impacts is that the differences in model simulations are relatively subtle in the majority of the cases examined. Several factors led to a limited impact of the GVF data on the model forecasts:

- Limited surface heating due to prevailing cloud cover and pre-existing precipitation,
- Strong synoptic dynamics that overwhelm differential surface heating,
- Overall poor model performance due to atmospheric initial condition uncertainty and/or random model errors.

The ideal case is one that consists of a reasonably accurate control model forecast along with little cloud cover and antecedent precipitation prior to the severe weather events. Such a scenario maximizes the contributions of differential sensible and latent heat fluxes due to variations in GVF and minimizes the contaminating effects of pre-existing clouds and precipitation systems.

Several cases experienced limited impact due largely to the reasons listed above. Strong synoptic forcing and/or prevailing clouds/precipitation resulted in nominal impact on 17 June 2010, 24-26 October 2010, and 27 April 2011. A general poor model performance occurred on 10-11 June 2010 and 15 June 2010 (location errors in convection and false alarm regions). On 24 May 2011, both the control and experimental model runs missed convective initiation altogether across western and central Oklahoma.

Out of all the simulated events, two cases stood out as having the most positive impact with the inclusion of the real-time MODIS GVFs: 17 July 2010 and 22 May 2011. These cases both exhibited substantial surface heating during the daytime, thereby maximizing the differences in surface fluxes and evapotranspiration, leading to changes in the evolution of simulated convection. A summary of the SPC severe reports for both these days is given in Figure 2. On 17 July 2010, numerous tornado, large hail, and severe wind reports occurred over eastern South Dakota, central Minnesota, and Iowa, which is the focus area subset for presenting model comparisons. On 22 May 2011, numerous tornadoes and hail/wind severe reports occurred from northeastern Oklahoma to northern Wisconsin. However, model sensitivity results are focused on a geographical subset centered on Joplin, MO.

##### 4.1 17 July 2010 case

In the Upper Midwest focus area, the pattern of GVF were broadly similar, but with notable differences. The High Plains from Nebraska to North Dakota generally had higher MODIS GVF up to 20% or more, while lower MODIS GVF occurred across western Illinois and northern Minnesota (Figure 3). A relative minimum in GVF over urban regions shows up more distinctly in the MODIS daily product.

This day featured an optimal scenario for examining the sensitivity of the model to the new GVF dataset in that surface heating was minimally impacted

by prevailing modeled cloud cover, as seen in the 19-h forecast total column condensate (combined cloud and precipitation microphysics) of Figure 4. Both the control and sportgvf runs produced very little cloudiness for the several hours of peak solar heating. Consequently, the differences in GVF translated almost directly into a change in the partitioning of the incoming shortwave radiation into sensible and latent heat fluxes. Regions of higher MODIS GVF from Nebraska to North Dakota (Figure 3) simultaneously led to a reduction in the sensible heat flux by  $50+ \text{ W m}^{-2}$  and an increase in latent heat flux up to  $100+ \text{ W m}^{-2}$  in the 19-h WRF forecast (Figure 5).

These modifications in the heat fluxes due to GVF translated to changes in the 21-h forecast 2-m temperature and dew point, as seen in Figure 6 and Figure 7. The western part of the focus area that had higher MODIS GVF (Figure 3) experienced a net decrease (increase) in the 2-m temperature (dew point), typically on the order of  $1-2^\circ$ , although local increases in dew point exceeded  $4^\circ\text{C}$  at 21 hours. The slightly lower 2-m temperatures in the sportgvf run over South Dakota are more in-line with the observations plotted in Figure 6; however, both model runs generally under-estimate the forecast 2-m temperatures over eastern Nebraska, and southern and western Iowa. Conversely, portions of northern Minnesota and western Illinois have the opposite response where the GVF was lower in the sportgvf run.

The net effect in the 21-h forecast (just prior to convective initiation) is an overall increase in the convective available potential energy (CAPE, Figure 8), especially over the western part of the focus area. Portions of eastern Nebraska to southeastern North Dakota had CAPE increases over  $1000 \text{ J kg}^{-1}$ . In this instance, the higher GVFs over the warm sector led to a greater influx of moisture into a shallower boundary layer (not shown), resulting in a net increase in moist static energy per unit mass within the boundary layer, despite small decreases in the 2-m temperature.

The impact of these GVF sensitivities to the model simulated precipitation was fairly subtle initially. Convective precipitation developed at 21 hours in both simulations over extreme southeastern North Dakota (not shown) and evolved into a bow-shaped line in southern Minnesota by 27 hours (Figure 9). The difference in the 1-h simulation precipitation at 27 hours (lower left of Figure 9) suggests that the sportgvf run is a bit slower and more intense than the control over southern Minnesota. Both simulations incorrectly produce a nearly continuous line of precipitation when the observed precipitation is actually more discrete in nature (lower-right panel). However, over the next several hours, the control simulation quickly moved the precipitation into northern Missouri, while the sportgvf run regenerates/back-builds convection more similar to the observed evolution. By 33-h (0900 UTC 18 July), the location and intensity of the sportgvf 1-h accumulated precipitation was more closely aligned with the Stage IV precipitation compared to the control run (Figure 10). This improved simulated precipitation during this time is likely due to the higher residual CAPE in the sportgvf run over eastern Nebraska and western Iowa during these forecast hours (not shown).

## 4.2 22 May 2011 case

The climatology and MODIS GVF on 22 May 2011 have similar broad-scale patterns in the focus region, with maximum GVF over the forests of eastern Oklahoma, northwestern Arkansas, and southern Missouri, and minimum GVF in the agricultural belt in the Mississippi River Valley (Figure 11). The largest differences between the control GVF and real-time MODIS GVF are the enhanced gradient in southeast Missouri, lower MODIS GVF in southern Arkansas, and a band of slightly higher MODIS GVF from northeast Texas to central Missouri (bottom of Figure 11).

The 22 May 2011 event was not quite as clean as 17 July 2010, as cloud cover and ongoing precipitation occurred across part of the interest area. The 17-h forecast of total column condensate at 1700 UTC shows that cloud cover prevailed across southern and eastern Arkansas, eastern Oklahoma, and along the convergent cloud band in eastern Kansas and northern Missouri associated with the approaching front (Figure 12). The overall cloud shield, however, is reduced in the sportgvf run at this time. The patterns of heat flux differences do not correlate cleanly with the GVF difference field, as in the 17 July 2010 case. Regions that had a reduction in cloud cover experienced a substantial increase in both sensible and latent heat flux, as one would expect (i.e. increase of 100–200+  $W m^{-2}$  in northeast and southern Arkansas, and parts of eastern Oklahoma and Kansas, Figure 13). The reduction in cloud cover over Arkansas is likely due to the lower GVF in the sportgvf model run, which provided a reduced rate of evapotranspiration into the boundary layer.

At the 21-h forecast just prior to initiation of the convection that affected Joplin, MO, the simulated CAPE fields depicted very high instability of 3000–4000+  $J kg^{-1}$  from southeast Oklahoma to southwest Missouri (Figure 14). The sportgvf run generally simulated slightly higher CAPE across much of Missouri, with the largest CAPE differences found over eastern Arkansas where the control run produced more convection than the sportgvf run (not shown).

Two hours later at 2300 UTC, both model simulations had a cluster of convective precipitation over southeast Kansas into southwest Missouri (top panels in Figure 15). However, precipitation rates were more intense in the sportgvf run at over 25  $mm h^{-1}$ , more closely aligned with the Stage IV precipitation analysis (bottom-right of Figure 15). Following the Joplin, MO tornadic event, the convective precipitation evolved into a bow-shaped squall line in northern Arkansas and southern Missouri by 0300 UTC (Figure 16). The control run moved the convection more quickly into Arkansas and did not simulate the bowed structure of the line as well as the sportgvf run. The sportgvf run also back-built the convection into far northeast Oklahoma, similar to the Stage IV precipitation analysis (bottom right of Figure 16). In addition, the sportgvf run reduced the false alarm precipitation region over central Arkansas at this time.

These two cases experienced some improvements in the simulated precipitation systems as a result of incorporating real-time MODIS GVF in place of the

monthly climatology GVF. These results are not typical of the numerous events simulated, but the favorable impacts indicate the potential for model improvements in some warm-season severe convective precipitation events.

## 5. SUMMARY AND FUTURE WORK

This paper presented a technique for assessing the impact of real-time MODIS GVF data on numerical forecasts of various severe weather episodes from 2010 and 2011. The NU-WRF modeling system was the tool of choice to incorporate the MODIS GVF into both the Land Information System and WRF model. The coupling between LIS and WRF within NU-WRF enabled a uniquely configured set of static and time-varying land surface model parameters to run identically in the LIS offline spin-up run, as well as the Advanced Research WRF model simulations. WRF simulations were initialized with the LIS offline output for any given event, and forecasts were made on a Continental U.S. domain with 4-km grid spacing, using an identical configuration as in the real-time WRF runs at NSSL.

Most severe weather events simulated did not see appreciable impacts or improvements by incorporating real-time MODIS GVF, often due to a poor control simulation, strong synoptic forcing that masks land-atmosphere interactions, or pre-existing clouds and precipitation. However, the two cases highlighted in this paper saw differential sensible and latent heat fluxes caused by the GVF differences, which led to notable improvements in the simulated convective precipitation. Results from the various simulations will continue to be analyzed for quantifying the impacts of real-time MODIS GVF and land surface model output incorporating the real-time GVF data. Validation of near-surface meteorological variables and quantitative precipitation forecasts will be conducted to measure the level of improvement in the model forecasts.

## 6. ACKNOWLEDGEMENTS/DISCLAIMER

This research was funded by Dr. Tsengdar Lee of the NASA Science Mission Directorate's Earth Science Division in support of the SPoRT program at the NASA MSFC, as well as funding provided by the NASA Modeling Analysis and Prediction Solicitation NNH08ZDA001N-MAP (PI: Peters-Lidard/GSFC). Computational resources for this work were provided by the NASA Center for Climate Simulation at the NASA Goddard Space Flight Center. Mention of a copyrighted, trademarked or proprietary product, service, or document does not constitute endorsement thereof by the authors, ENSCO Inc., the University of Missouri, Raytheon, the SPoRT Center, the National Aeronautics and Space Administration, or the United States Government. Any such mention is solely for the purpose of fully informing the reader of the resources used to conduct the work reported herein.

## 7. REFERENCES

- Barlage, M., X. Zeng, H. Wei, and K. E. Mitchell, 2005: A global 0.05° maximum albedo dataset of snow-covered land based on MODIS observations. *Geophys. Res. Lett.*, **32**, L17405, doi:10.1029/2005GL022881.
- Bell, J. R., J. L. Case, F. J. LaFontaine, and S. V. Kumar, 2012: Evaluating the impacts of NASA/SPoRT daily greenness vegetation fraction on land surface model and numerical weather forecasts. Preprints, *16<sup>th</sup> Symp. on Integrated Observing and Assimilation Systems for the Atmosphere, Oceans, and Land Surface*, New Orleans, LA, Amer. Meteor. Soc., P247.
- Briegleb, B. P., P. Minnis, V. Ramanathan, and E. Harrison, 1986: Comparison of regional clear-sky albedos inferred from satellite observations and model computations. *J. Climate Appl. Meteor.*, **25**, 214-226.
- Case, J. L., W. L. Crosson, S. V. Kumar, W. M. Lapenta, and C. D. Peters-Lidard, 2008: Impacts of High-Resolution Land Surface Initialization on Regional Sensible Weather Forecasts from the WRF Model. *J. Hydrometeorol.*, **9**, 1249-1266.
- Case, J. L., F. J. LaFontaine, S. V. Kumar, and G. J. Jedlovec, 2011a: A real-time MODIS vegetation composite for land surface models and short-term forecasting. Preprints, *15<sup>th</sup> Symp. on Integrated Observing and Assimilation Systems for the Atmosphere, Oceans, and Land Surface*, Seattle, WA, Amer. Meteor. Soc., 11.2. [Available online at [http://ams.confex.com/ams/91Annual/webprogram/Manuscript/Paper180639/Case\\_etal\\_2011AMS-15IOAS-AOLS\\_11.2\\_FINAL.pdf](http://ams.confex.com/ams/91Annual/webprogram/Manuscript/Paper180639/Case_etal_2011AMS-15IOAS-AOLS_11.2_FINAL.pdf)]
- Case, J. L., S. V. Kumar, J. Srikishen, and G. J. Jedlovec, 2011b: Improving numerical weather predictions of summertime precipitation over the southeastern U.S. through a high-resolution initialization of the surface state. *Wea. Forecasting*, **26**, 785-807.
- Chen, F., and J. Dudhia, 2001: Coupling an advanced land-surface/hydrology model with the Penn State/NCAR MM5 modeling system. Part I: Model description and implementation. *Mon. Wea. Rev.*, **129**, 569-585.
- Cosgrove, B. A., and Coauthors, 2003: Real-time and retrospective forcing in the North American Land Data Assimilation System (NLDAS) project. *J. Geophys. Res.*, **108(D22)**, 8842, doi:10.1029/2002JD003118, 2003.
- Darden, C. B., D. J. Nadler, B. C. Carcione, R. J. Blakeslee, G. T. Stano, and D. E. Buechler, 2010: Utilizing total lightning information to diagnose convective trends. *Bull. Amer. Meteor. Soc.*, **91**, 167-175.
- Derber, J. C., D. F. Parrish, and S. J. Lord, 1991: The new global operational analysis system at the National Meteorological Center. *Wea. Forecasting*, **6**, 538-547.
- Ek, M. B., K. E. Mitchell, Y. Lin, E. Rogers, P. Grunmann, V. Koren, G. Gayno, and J. D. Tarpley, 2003: Implementation of Noah land surface model advances in the National Centers for Environmental Prediction operational mesoscale Eta model. *J. Geophys. Res.*, **108 (D22)**, 8851, doi:10.1029/2002JD003296.
- Friedl, M. A., D. Sulla-Menashe, B. Tan, A. Schneider, N. Ramankutty, A. Sibley, and X. Huang, 2010: MODIS Collection 5 global land cover: Algorithm refinements and characterization of new datasets. *Remote Sens. Environ.*, **114**, 168-182.
- Fuell, K. K., M. Smith, and G. J. Jedlovec, 2012: Early transition and use of NPP/VIIRS and GOES-R ABI and GLM products by NWS forecast offices. Preprints, *Eighth Annual Symposium on Future Operational Environmental Satellite Systems*, New Orleans, LA, Amer. Meteor. Soc., 5.4.
- Gutman, G. and A. Ignatov, 1998: Derivation of green vegetation fraction from NOAA/AVHRR for use in numerical weather prediction models. *Int. J. Remote Sensing*, **19**, 1533-1543.
- Haines, S. L., G. J. Jedlovec, and S. M. Lazarus, 2007: A MODIS sea surface temperature composite for regional applications. *IEEE Trans. Geosci. Remote Sens.*, **45**, 2919-2927.
- James, K. A., D. J. Stensrud, and N. Yussouf, 2009: Value of real-time vegetation fraction to forecasts of severe convection in high-resolution models. *Wea. Forecasting*, **24**, 187-210.
- Janjic, Z. I., 2003: A Nonhydrostatic Model Based on a New Approach. *Meteorology and Atmospheric Physics*, **82**, 271-285.
- Janjic, Z. I., J. P. Gerrity, Jr. and S. Nickovic, 2001: An Alternative Approach to Nonhydrostatic Modeling. *Mon. Wea. Rev.*, **129**, 1164-1178.
- Jiang, L., and Coauthors, 2010: Real-time weekly global green vegetation fraction derived from advanced very high resolution radiometer-based NOAA operational global vegetation index (GVI) system. *J. Geophys. Res.*, **115**, D11114, doi:10.1029/2009JD013204.
- Kain, J. S., S. R. Dembek, S. J. Weiss, J. L. Case, J. J. Levitt, and R. A. Sobash, 2010: Extracting unique information from high-resolution forecast models: Monitoring selected fields and phenomena every time step. *Wea. Forecasting*, **25**, 1536-1542.
- Kumar, S. V., and Coauthors, 2006. Land Information System – An Interoperable Framework for High Resolution Land Surface Modeling. *Environmental Modeling & Software*, **21 (10)**, 1402-1415, doi:10.1016/j.envsoft.2005.07.004.
- Kumar, S. V., C. D. Peters-Lidard, J. L. Eastman, and W.-K. Tao, 2007: An integrated high-resolution hydrometeorological modeling testbed using LIS

- and WRF. *Environmental Modeling & Software*, **23** (2), 169-181, doi: 10.1016/j.envsoft.2007.05.012.
- Kurkowski, N. P., D. J. Stensrud, and M. E. Baldwin, 2003: Assessment of implementing satellite-derived land cover data in the Eta model. *Wea. Forecasting*, **18**, 404-416.
- Loveland, T. R., B. C. Reed, J. F. Brown, D. O. Ohlen, Z. Zhu, L. Yang, and J. W. Merchant, 2000: Development of a global land cover characteristics database and IGBP DISCover from 1 km ABHRR data. *Int. J. Remote Sensing*, **21**, 1303-1330.
- Miller, D. A. and R. A. White, 1998: A Conterminous United States multi-layer soil characteristics data set for regional climate and hydrology modeling. *Earth Interactions*, 2. [Available on-line at <http://EarthInteractions.org>].
- Miller, J. M. Barlage, X. Zeng, H. Wei, K. Mitchell, and D. Tarpley, 2006: Sensitivity of the NCEP/Noah land surface model to the MODIS green vegetation fraction data set. *Geophys. Res. Lett.*, **33**, L13404, doi:10.1029/2006GL026636.
- Skamarock, W. C., J. B. Klemp, J. Dudhia, D. O. Gill, D. M. Barker, M. G. Duda, X-Y. Huang, W. Wang and J. G. Powers, 2008: A Description of the Advanced Research WRF Version 3, NCAR Technical Note, NCAR/TN-475+STR, 123 pp. [Available on-line at: [http://www.mmm.ucar.edu/wrf/users/docs/arw\\_v3.pdf](http://www.mmm.ucar.edu/wrf/users/docs/arw_v3.pdf)]
- Stano, G. T., 2012: Evaluation of NASA SPoRT's Pseudo-Geostationary Lightning Mapper Products in the 2011 Spring Program. Preprints, *Eighth Annual Symposium on Future Operational Environmental Satellite Systems*, New Orleans, LA, Amer. Meteor. Soc., P501.

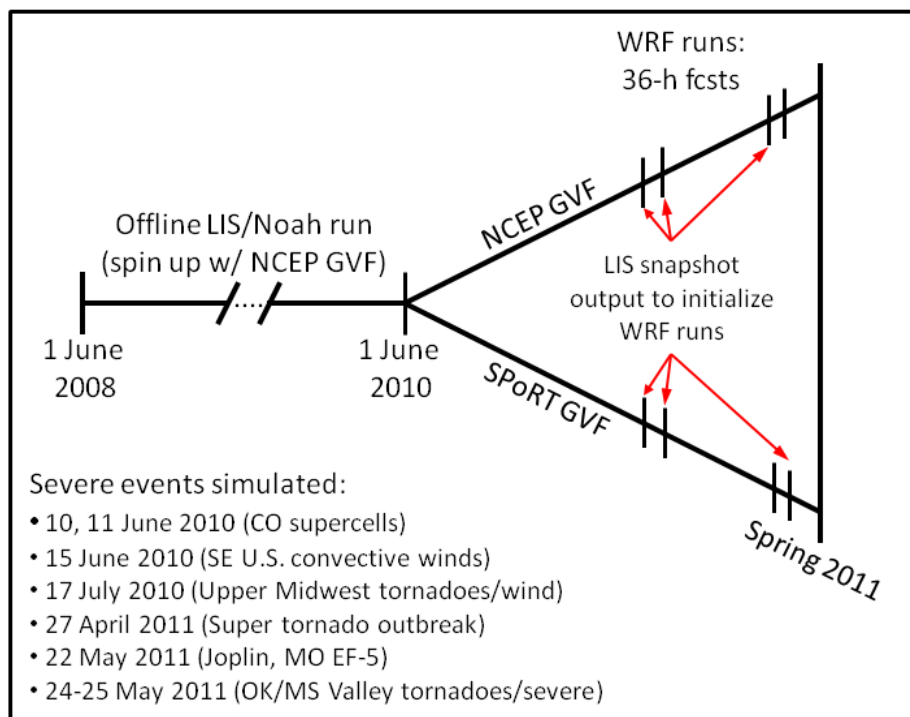


**Figure 1. Methodology for spinning up the land surface fields within the LIS/Noah offline run, followed by the split into control (top line) and experimental (bottom line) LIS offline runs. Severe weather case dates listed were initialized using LIS land surface fields and the accompanying NCEP or MODIS GVF.**

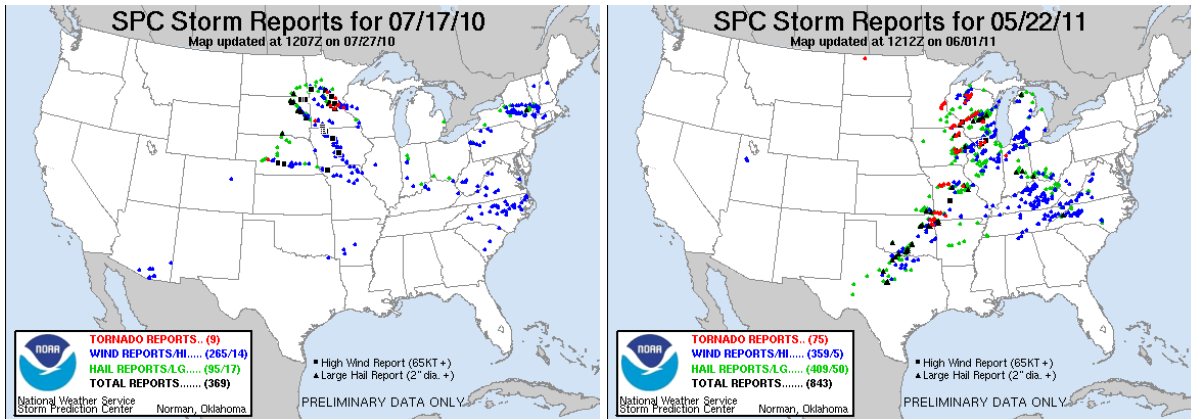


Figure 2. Storm Prediction Center (SPC) storm reports from 17 July 2010 (left), and 22 May 2011 (right).

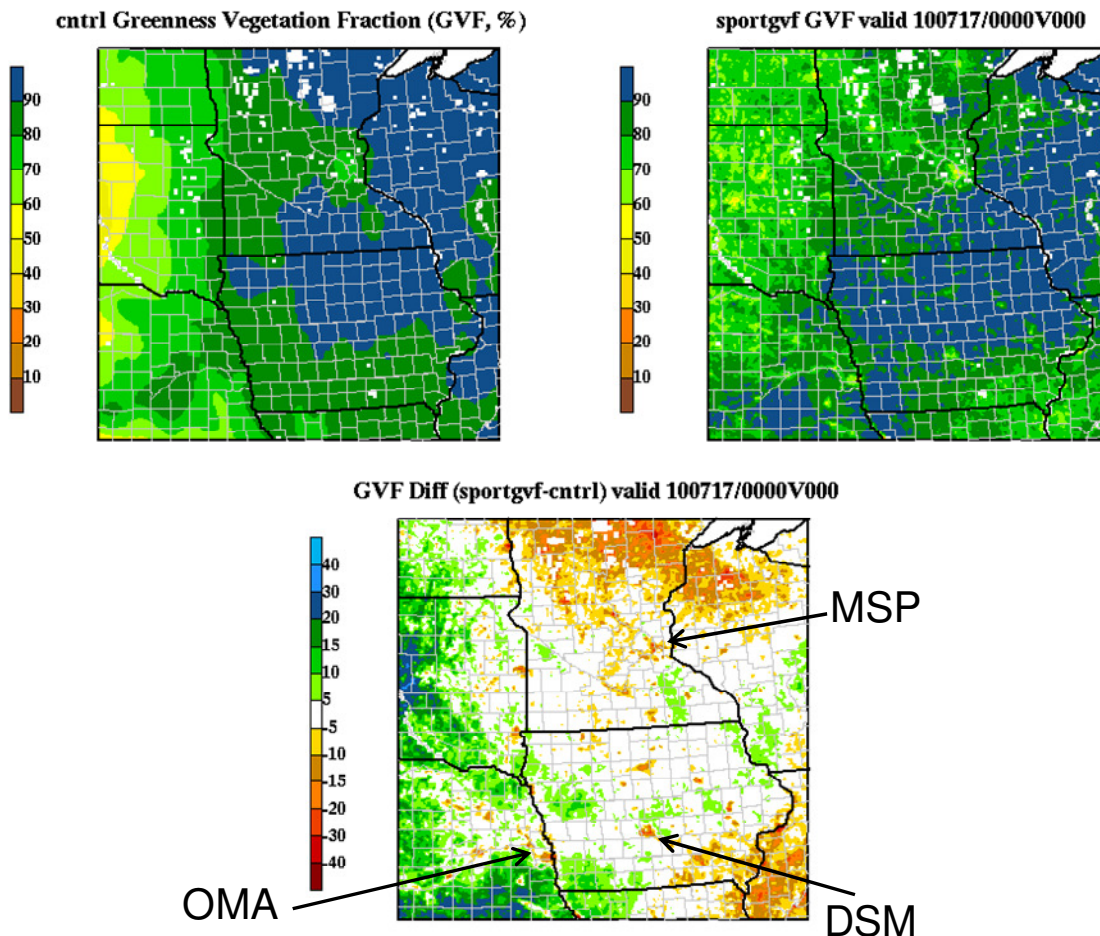
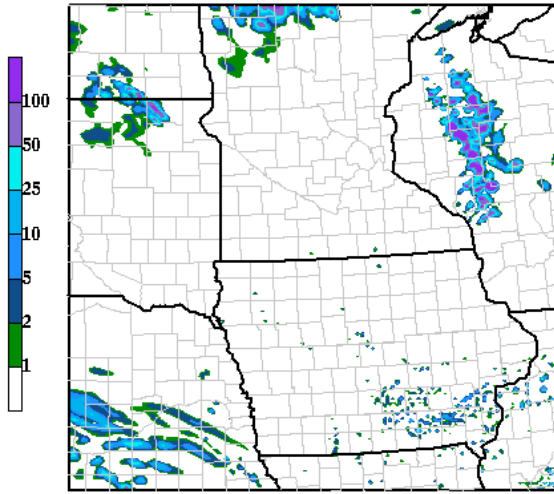


Figure 3. Comparison of the greenness vegetation fraction (GVF) in the 17 July 2010 simulations, depicting NCEP climatology GVF in the control simulation (upper-left), SPoRT/MODIS GVF in the experimental simulation (upper-right), and difference in GVF (SPoRT – NCEP, bottom panel).

cntrl TCol Condensate (\*10\*\*2) valid 100717/1900V019



sportgvf TCol Condensate valid 100717/1900V019

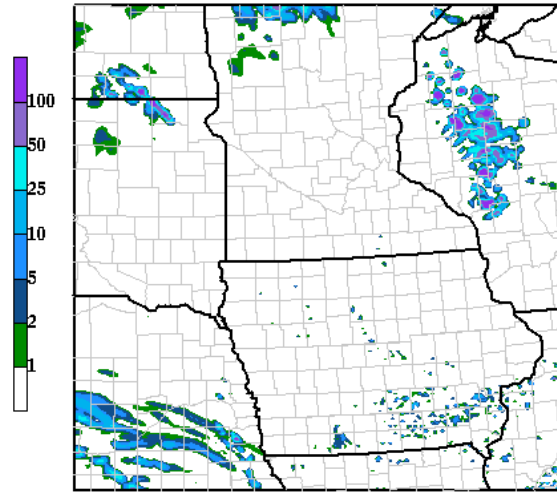
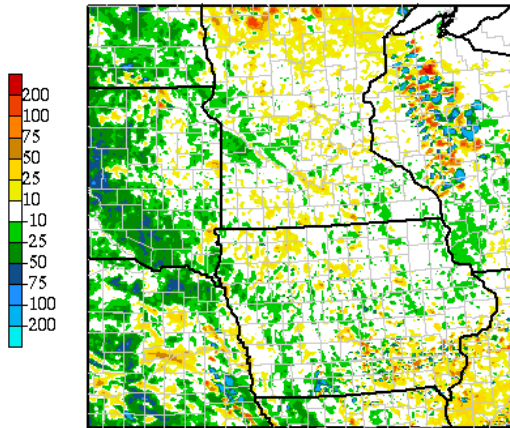


Figure 4. Total column cloud and precipitation condensate ( $\text{g kg}^{-1}$ ) for the 19-h forecast valid 1900 UTC 17 July 2010 for the control run (left) and sportgvf experimental run (right).

Sensible HF Diff (sportgvf-cntrl) valid 100717/1900V019



Latent HF Diff (sportgvf-cntrl) valid 100717/1900V019

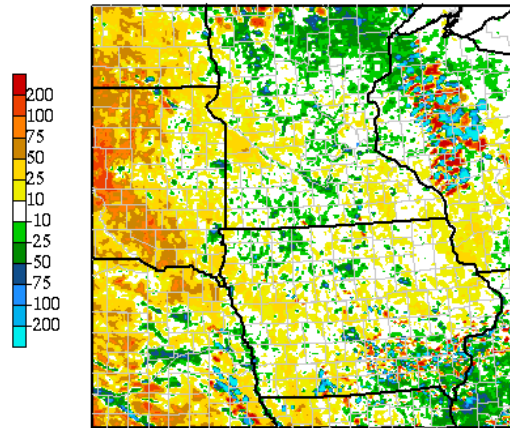
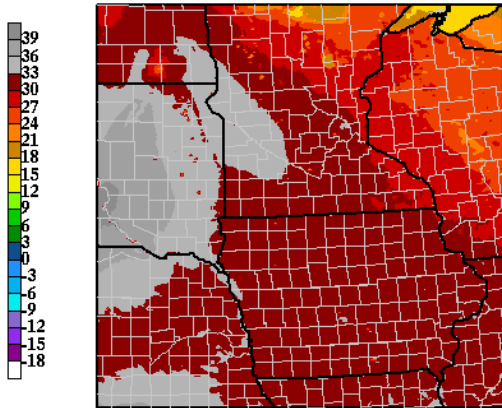
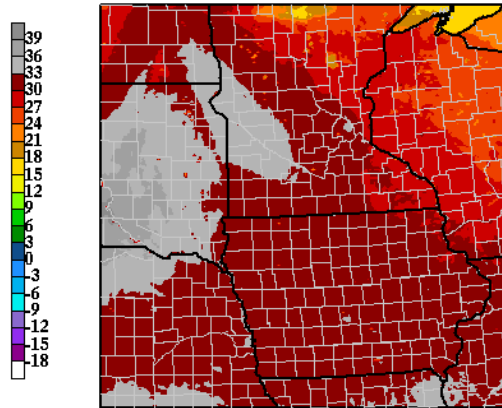


Figure 5. Difference in sensible (left) and latent heat flux (right, sportgvf – control in  $\text{W m}^{-2}$ ) for the 19-h forecast valid 1900 UTC 17 July 2010.

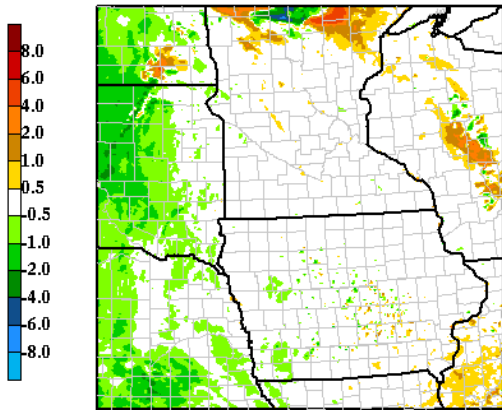
cntrl 2-m Temperature (C) valid 100717/2100V021



sportgvf 2-m Temperature (C) valid 100717/2100V021



2-m Temp Diff (sportgvf-cntrl) valid 100717/2100V021



Observed 2-m Temperature at 100717/2100

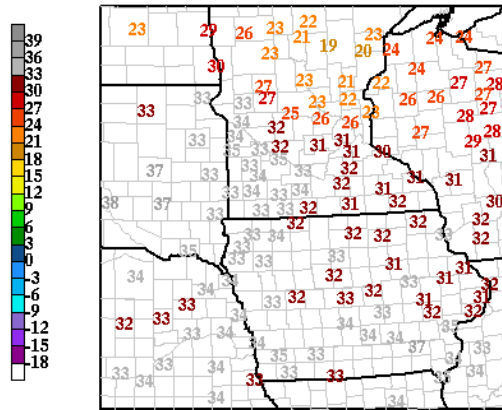
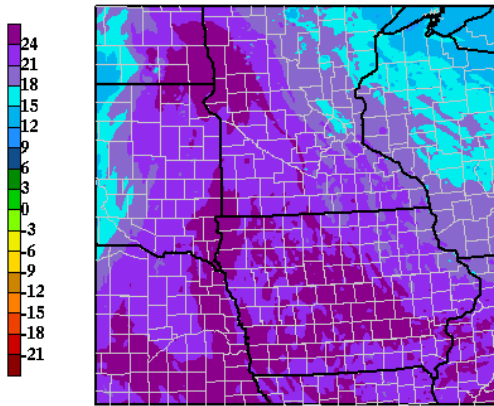
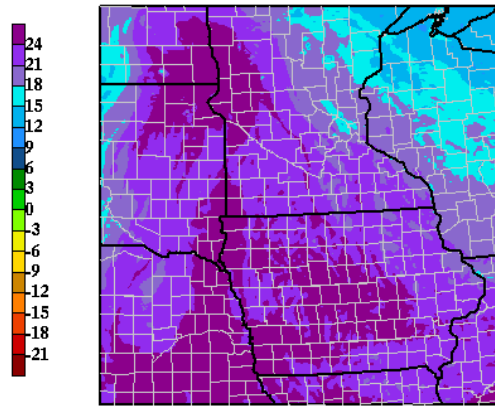


Figure 6. NU-WRF 21-h forecast 2-m temperature in °C for the control run (upper-left), sportgvf run (upper-right), difference (lower-left, sportgvf – control), and observed 2-m temperature (lower-right), valid 2100 UTC 17 July 2010, just prior to convective initiation.

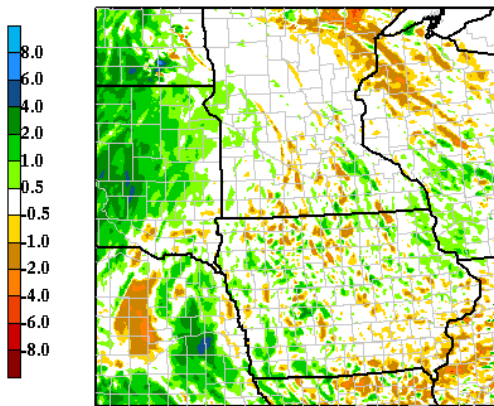
cntrl 2-m Dewpoints (C) valid 100717/2100V021



sportgvf 2-m Dewpoints (C) valid 100717/2100V021



2-m Dewp Diff (sportgvf-cntrl) valid 100717/2100V021



Observed 2-m Dewpoint at 100717/2100

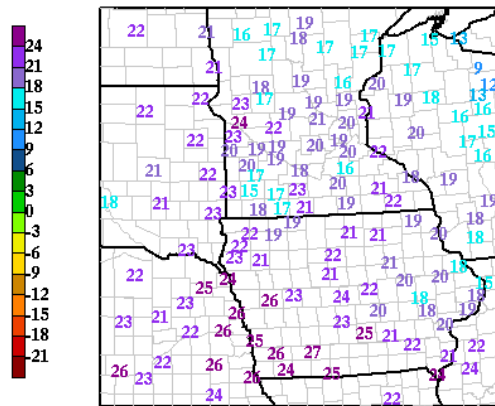


Figure 7. Same as in Figure 6, except for the 2-m dew point temperature.

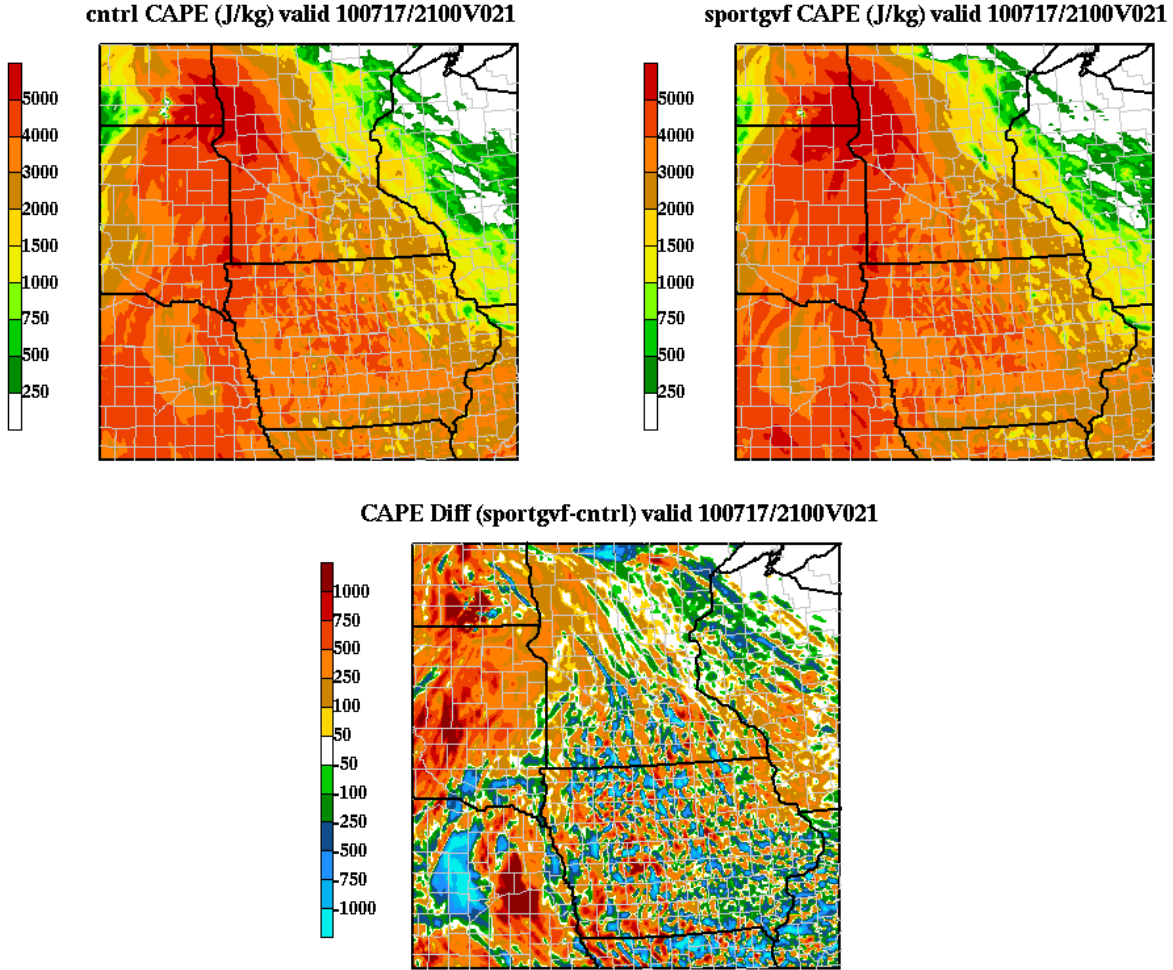


Figure 8. NU-WRF 21-h forecast convective available potential energy (CAPE,  $\text{J kg}^{-1}$ ) for the control run (upper-left), sportgvf run (upper-right), and difference (bottom, sportgvf – control), valid 2100 UTC 17 July 2010, just prior to convective initiation.

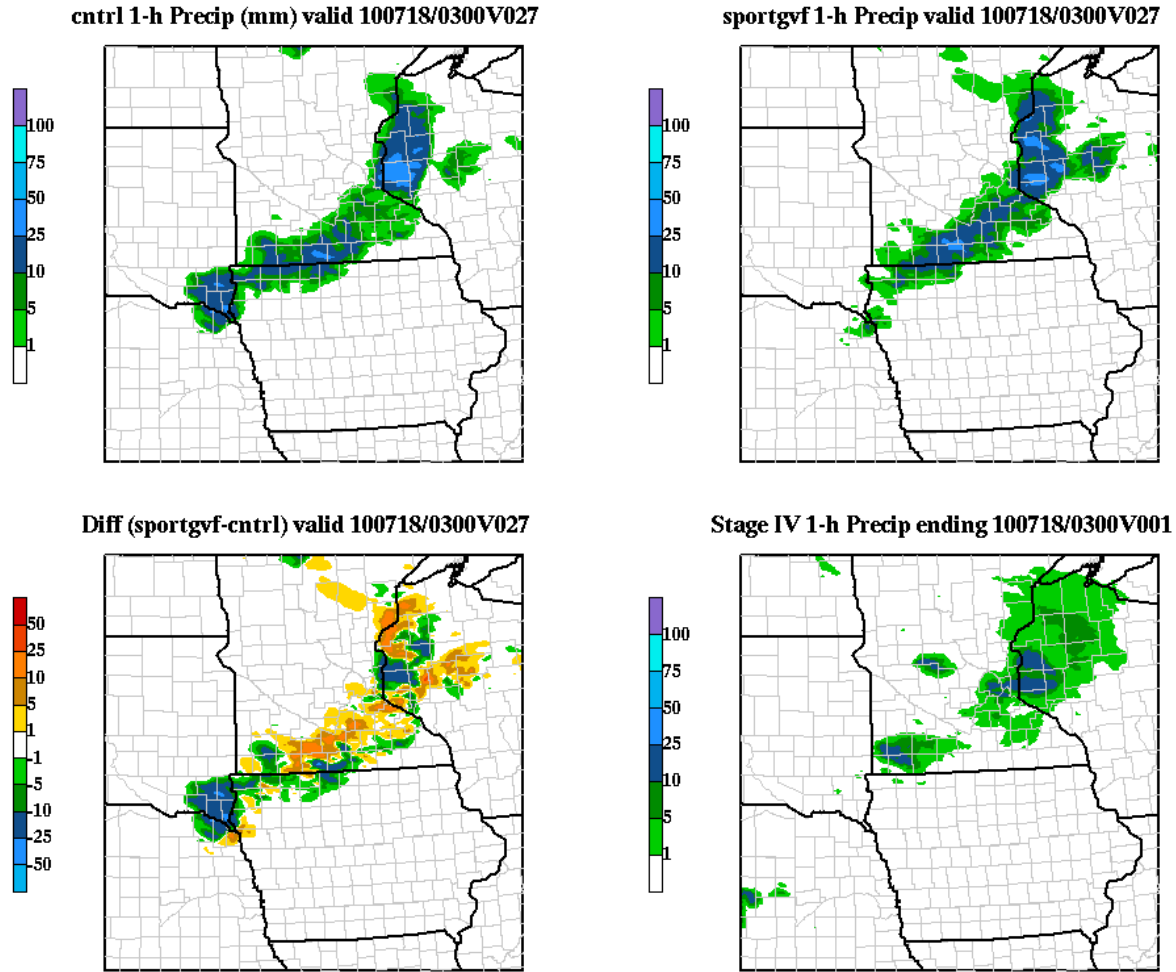
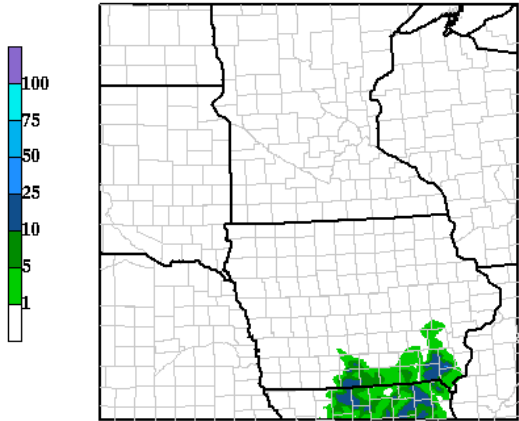
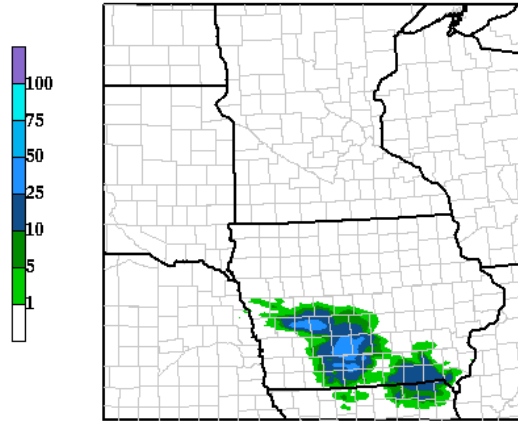


Figure 9. NU-WRF 1-h accumulated precipitation (mm) for the 27-h forecast of the control run (upper-left), sportgvf run (upper-right), difference (bottom-left, sportgvf – control), and stage IV precipitation analysis, valid for the hour ending 0300 UTC 18 July 2010.

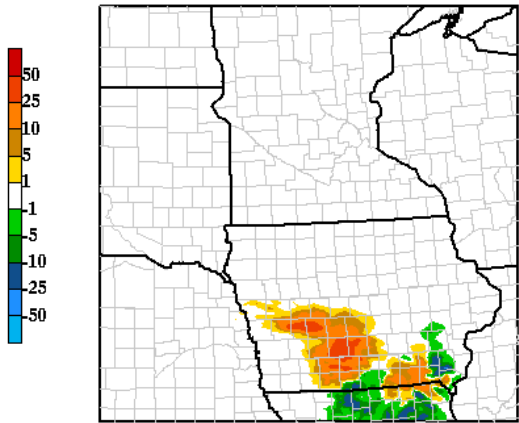
cntrl 1-h Precip (mm) valid 100718/0900V033



sportgvf 1-h Precip valid 100718/0900V033



Diff (sportgvf-cntrl) valid 100718/0900V033



Stage IV 1-h Precip ending 100718/0900V001

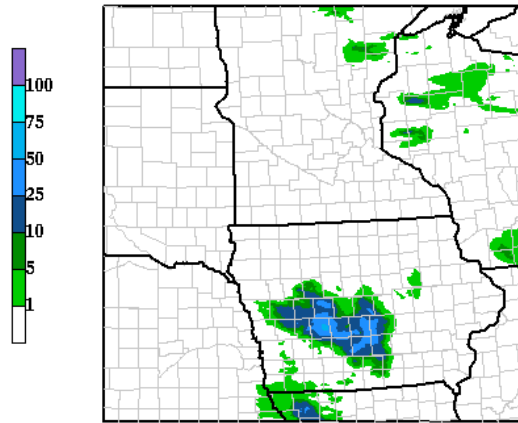


Figure 10. Same as in Figure 9, except for the 33-h forecast for the hour ending 0900 UTC 18 July 2010.

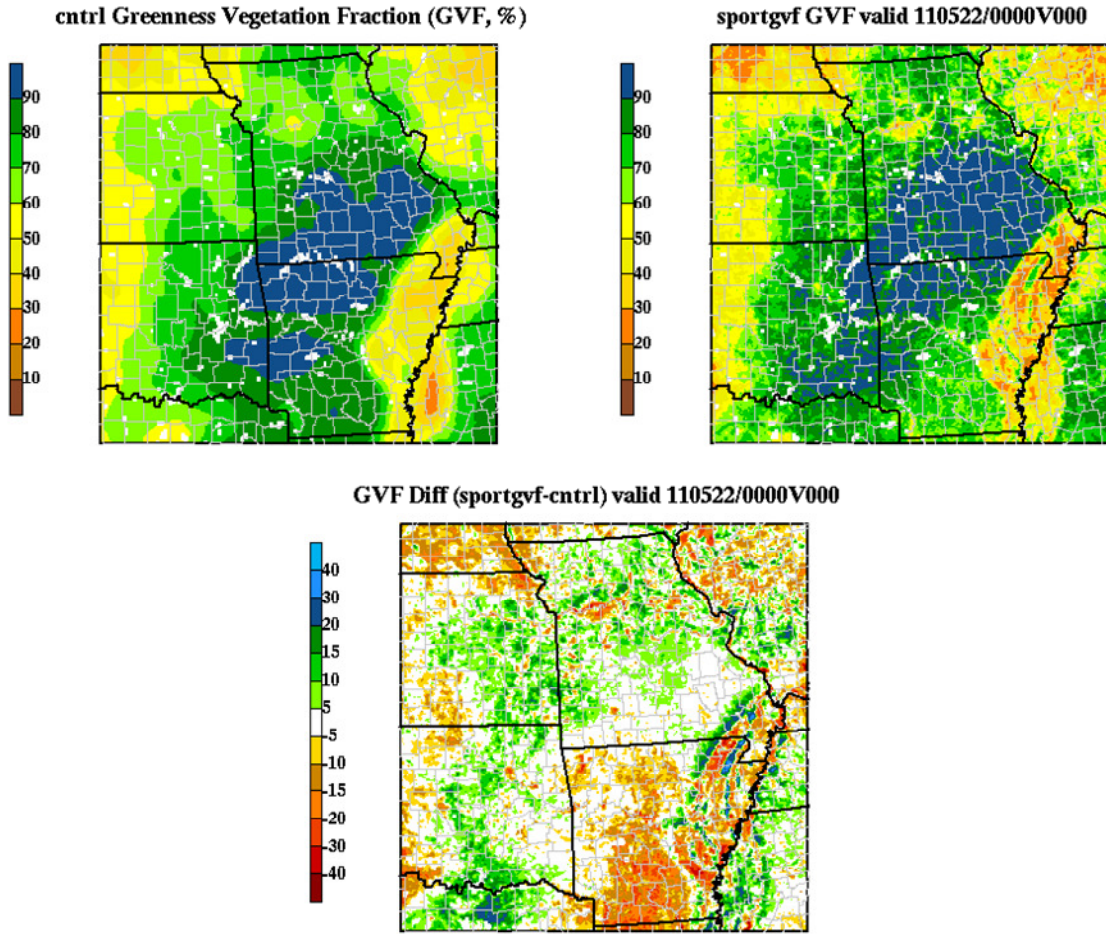


Figure 11. Same as in Figure 3, except for the 22 May 2011 simulations.

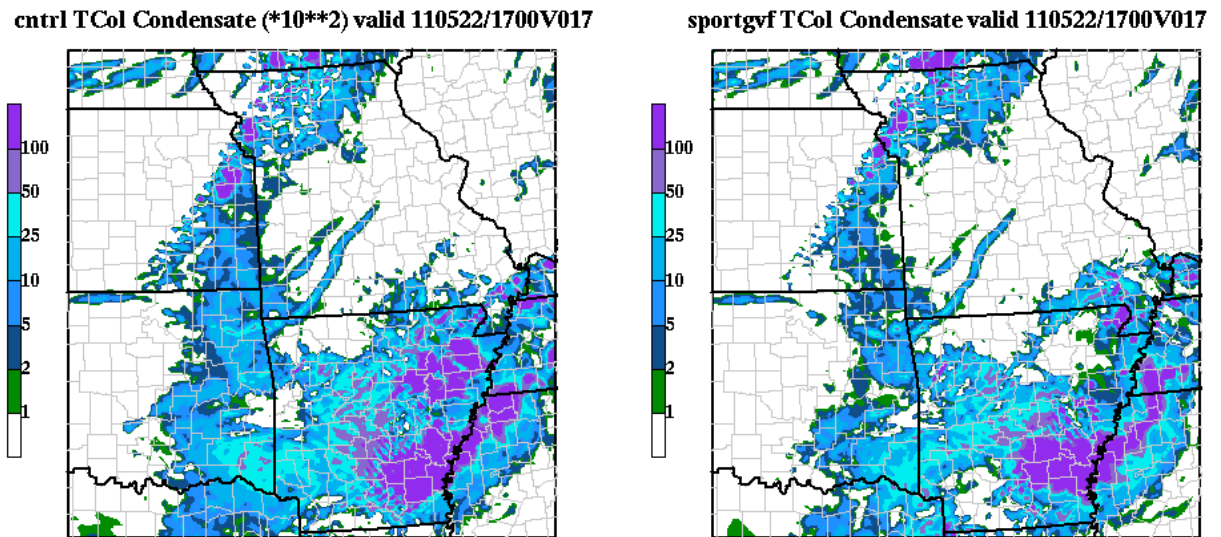
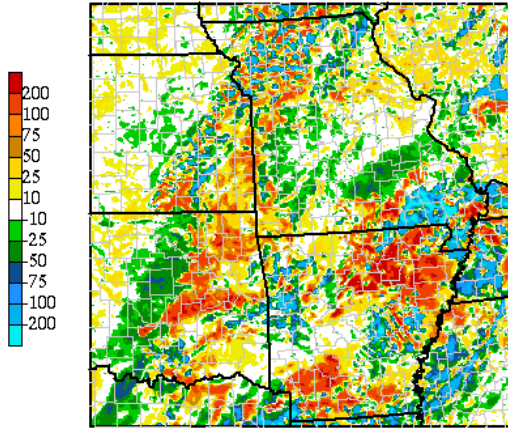


Figure 12. Same as in Figure 4, except for the 17-h forecast from the 22 May 2011 simulations, valid 1700 UTC.

Sensible HF Diff (sportgvf-cntrl) valid 110522/1700V017



Latent HF Diff (sportgvf-cntrl) valid 110522/1700V017

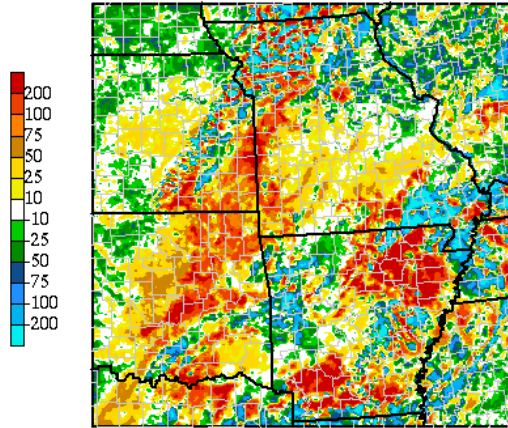
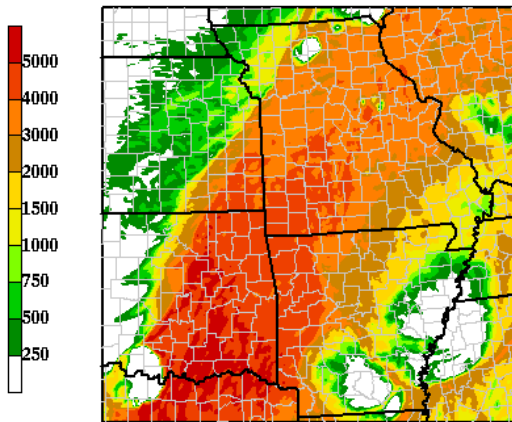
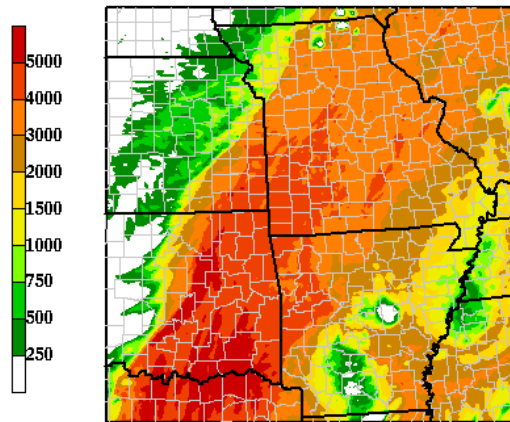


Figure 13. Same as in Figure 5, except for the 17-h forecast from the 22 May 2011 simulations, valid 1700 UTC.

cntrl CAPE (J/kg) valid 110522/2100V021



sportgvf CAPE (J/kg) valid 110522/2100V021



CAPE Diff (sportgvf-cntrl) valid 110522/2100V021

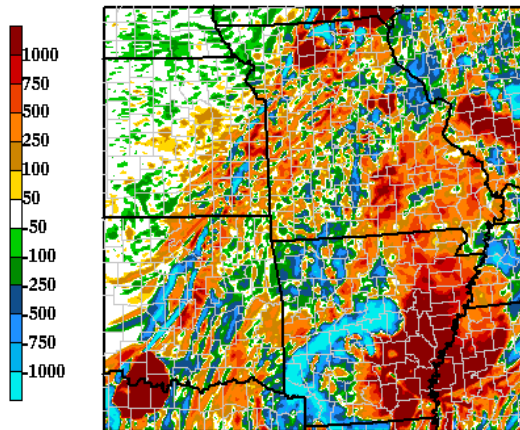
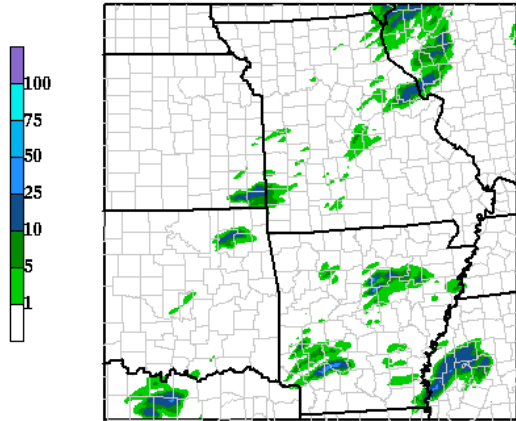
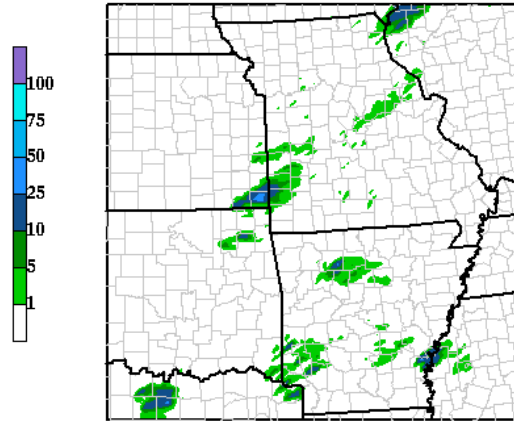


Figure 14. NU-WRF 21-h forecast CAPE ( $\text{J kg}^{-1}$ ) for the control run (upper-left), sportgvf run (upper-right), and difference (bottom, sportgvf – control), valid 2100 UTC 22 May 2011, just prior to the initiation of convection that impacted Joplin, MO.

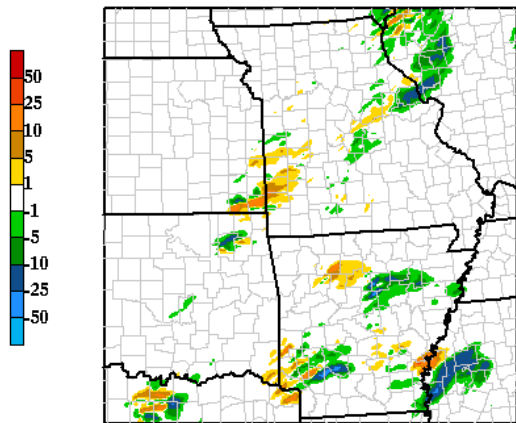
cntrl 1-h Precip (mm) valid 110522/2300V023



sportgvf 1-h Precip valid 110522/2300V023



Diff (sportgvf-cntrl) valid 110522/2300V023



Stage IV 1-h Precip ending 110522/2300V001

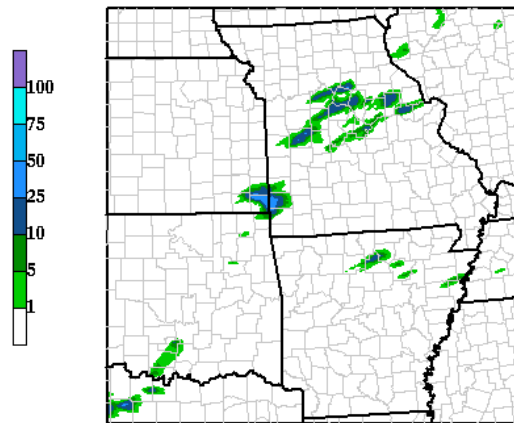
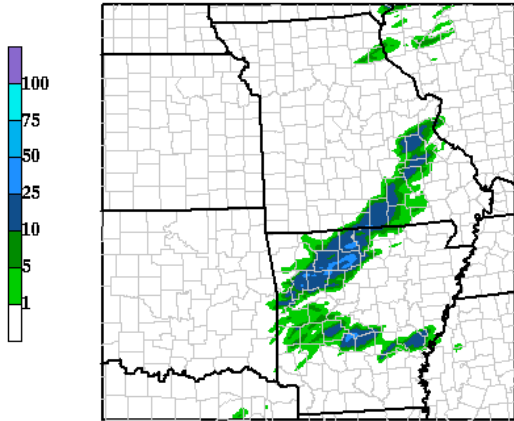
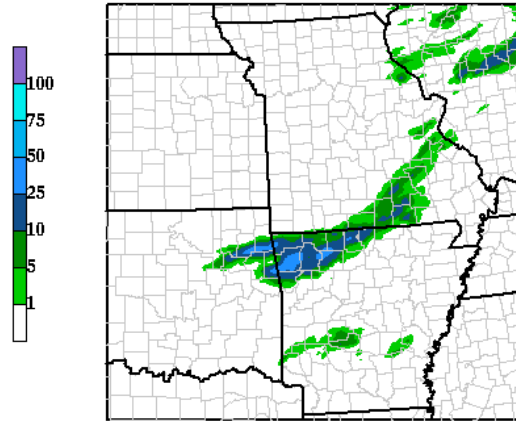


Figure 15. NU-WRF 1-h accumulated precipitation (mm) for the 23-h forecast of the control run (upper-left), sportgvf run (upper-right), difference (bottom-left, sportgvf – control), and stage IV precipitation analysis, valid for the hour ending 2300 UTC 22 May 2011.

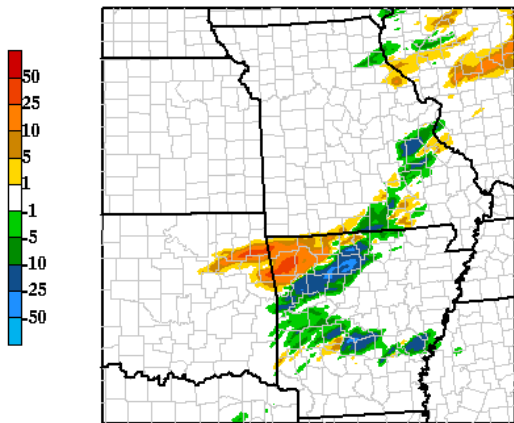
cntrl 1-h Precip (mm) valid 110523/0300V027



sportgvf 1-h Precip valid 110523/0300V027



Diff (sportgvf-cntrl) valid 110523/0300V027



Stage IV 1-h Precip ending 110523/0300V001

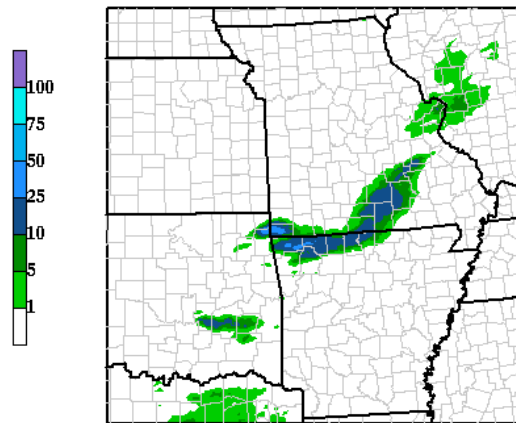


Figure 16. Same as in Figure 15, except for the 27-h forecast for the hour ending 0300 UTC 22 May 2011.